New Method to Quantify the Operation Condition for Zone 3 Impedance Relays during Low-Frequency Power Swings

Shenghu Li*

Abstract – With long time setting, zone 3 impedance relays are considered insensitive to pow er swings, and their operation condition during power swings is seldom analyzed. Instead of ti me-consuming simulation to the swing loci, their operation condition is directly quantified by polynominal functions in this paper to find the critical swing angle and frequency for relay op eration under different relay settings and system parameters. It is found: (1) the swing loci are more densely populated inside than outside of the protection region, which corresponds to lon g residence time and possible relay operations; (2) the relays may be sensitive to load encroac hments and stable power swings with different relay settings and system parameters; (3) the cr itical swing frequency may be in the range of low-frequency power swings.

Keywords: Load modeling, Parameter, Traction power supply system

1. Nomenclature

$\bar{E}_M$,$\bar{E}_N$	Equivalent source voltages.
f_{sw}	Swing frequency.
$\bar{Z}_M=Z_M e^{j\varphi M}$	Impedance of source M.
$\bar{Z}_N=Z_N e^{j\varphi N}$	Impedance of source N.
$\bar{I}_L$	Line current at relay's location.
$\bar{Z}_L=Z_L e^{j\varphi L}$	Impedance of the protected line.
$\bar{Z}_\Sigma=Z_\Sigma e^{j\varphi\Sigma}$	Total impedance on the swing path.
$\bar{Z}_a=Z_a e^{j\varphi a}$	Apparent impedance of the impedance relay.
$\bar{Z}_R=Z_R\angle\varphi_T$	Setting of zone 3 impedance relay.
Z_{op}	Operation impedance of the relay.

2. Introduction

Power swings, i.e. electro-mechanical oscillations among synchronous generators, are caused by load surges, faults, line switching, and excitation and regulation controls, etc. Their frequency may be in the range of 0.1-2.0 Hz [1]. The apparent impedance seen by the impedance relays during power swing possibly enter their protection region, leading to transient instability and cascading tripping [2, 3].

For faults or faults during power swings, the relays are expected to operate. For stable power swings, Power Swing Blocking (PSB) stops the relays from operation according to the three-phase symmetry and the speed of the impedance loci. For unstable swings, Out-of-Step Tripping (OST) separates the system into islands near the swing center to avoid major blackouts [4, 5]. Usually PSB and OST are not designed for zone 3 relays, which are considered insensitive to power swings for their long time setting, e.g. in the order of several tenths of seconds to a few seconds [6].

However, the protection region of zone 3 relays includes those of zone 1 and 2, and their vulnerability to the system conditions [7–10]. Therefore, for zone 3 relays (mho) without PSB and OST, the operation condition for the zone 3 relays to power swings has not yet been fully studied, such as:

(i) Influence of relay setting and system parameters on the relay performance during power swings [11–13]. For example, the Maximum Torque Angle (MTA) may be set less than the line impedance angle to improve its dependability to high impedance faults, or close to $\pi/2$ to avoid maloperation of the impedance relays under load encroachment.

(ii) For the bulk power system with extra or ultra high voltages [14, 15], the swing frequency may be low enough to satisfy the time setting, and activate the zone 3 relays.

In this paper, the operation condition of zone 3 impedance relays during power swings is newly expressed to quantify the critical swing angle and frequency.

* School of Electrical Engineering and its Automation, Hefei University of Technology, China. (e-mail: lishenghu2004@hotmail.com).
Received 26 April, 2007 ; Accepted 2 November, 2007

Numerical results show that the operation condition for zone 3 impedance relays is closely dependent on relay setting and system parameters, and the critical swing frequency may be in the range of low-frequency power swings.

3. Operation condition of impedance relays during power swings

An equivalent power system with 2 aggregated generators and one transmission line is shown in Fig. 1, where the source voltages follow $\bar{E}_M/\bar{E}_N=\bar{K}=K\angle\delta$, $-\pi\le\delta\le\pi$. Two assumptions are made to quantify the relay performance:

(i) The transmission lines are fully transposed, and power swings are three-phase balanced.

(ii) Source impedances and line impedance keep constant with the variation of system frequency.

As shown in Fig. 2, for a practical K, the swing locus is a circle whose radius is much longer than the relay setting. The swing locus inside of the protection region is longer than that outside, i.e. $\overset{\frown}{abc}\ll\overset{\frown}{cda}$. However as revealed in Section V, part A., the residence time inside the protection region, is not proportional to the length of the swing loci.

If swing frequency f_{sw} is approximately constant, the time condition for relay operation is given by (1), where t_{op} is the time setting for the relay and δ_1 and δ_2 are the swing angles traversing into and out of the protection region. The critical frequency leading to relay operation is given by (2). When f_{sw} is lower than the critical value $f_{sw,cr}$, the relay will be activated.

$$\Delta t\approx\frac{\Delta\delta}{2\pi f}>t_{op},\ \Delta\delta=2\pi+\delta_2-\delta_1 \tag{1}$$

$$f_{sw}<f_{sw,cr}=\frac{\Delta\delta}{2\pi}\frac{1}{t_{op}} \tag{2}$$

It is time-consuming to search the critical swing angles by simulating the swing loci continually for a specified system. A direct method helps to quantify the relay operation condition, as well as the influence from the relay setting and the system parameters.

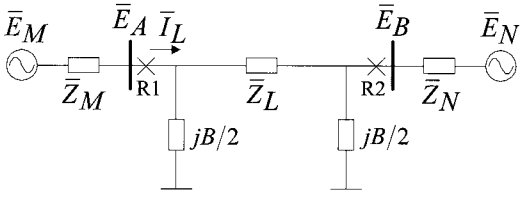

Fig. 1. Equivalent system for power swing studies

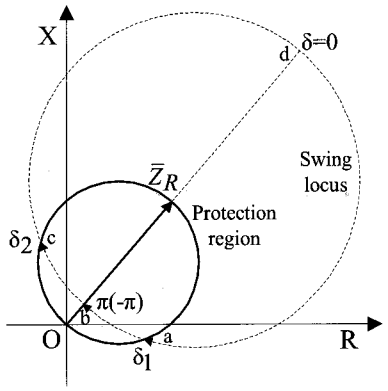

Fig. 2. Residence time of swing loci inside the protection region

4. Critical swing angle during power swings

4.1 Without considering source impedances

When the source impedances and the line capacitance are neglected, the total impedance on the swing path is equal to the line impedance (3). The apparent and the operation impedance for relay R1 are given by (4) and (5). As indicated in Fig. 3, the apparent impedance leads the line impedance for a negative δ, and lags for a positive δ.

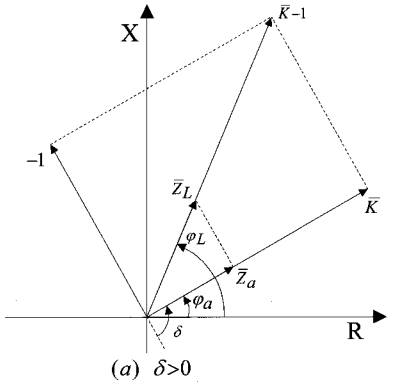

(a) $\delta>0$

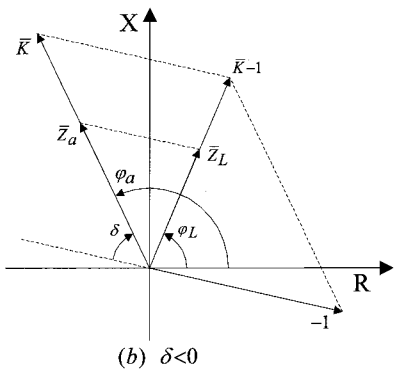

(b) $\delta<0$

Fig. 3. Apparent impedance without source impedances and shunt capacitance

$$\bar{Z}_\Sigma=\bar{Z}_M+\bar{Z}_L+\bar{Z}_N\approx\bar{Z}_L \tag{3}$$

$$\bar{Z}_a=\frac{\bar{E}_A}{\bar{I}_L}\approx\frac{\bar{E}_M\bar{Z}_L}{\bar{E}_M-\bar{E}_N}=\frac{Z_L K}{\sqrt{K^2-2K\cos\delta+1}}\angle\left(\varphi_{line}+\delta-\text{atan}\frac{K\sin\delta}{K\cos\delta-1}\right) \tag{4}$$

$$Z_{op}=Z_R\cos(\varphi_T-\varphi_a) \tag{5}$$

The operation condition given by $Z_a-Z_{op}<0$ is expanded to (6), which is rewritten in terms of K or δ in (7) and (8).

$$\left[Z_R\cos(\varphi_T-\varphi_L)-Z_L\right]K>Z_R\cos(\varphi_T-\varphi_L-\delta) \tag{6}$$

$$Z_R\cos(\varphi_T-\varphi_L)-Z_L>0,\ K>\frac{Z_R\cos(\varphi_T-\varphi_L-\delta)}{Z_R\cos(\varphi_T-\varphi_L)-Z_L} \tag{7}$$

$$|\varphi_T-\varphi_L-\delta|>\text{acos}\frac{\left[Z_R\cos(\varphi_T-\varphi_L)-Z_L\right]K}{Z_R} \tag{8}$$

4.2 With source impedances

With source impedances, the apparent impedance is given by (9), where λ_r and λ_i are its real and imaginary parts respectively. As seen in Fig. 4, due to the inductive source impedances, the apparent impedance leads the line impedance more for a negative δ, and lags more for a positive δ. The operation impedances are given by (10).

$$\bar{Z}_a=\frac{\bar{E}_A}{\bar{I}_L}=\frac{\bar{E}_M\bar{Z}_\Sigma}{\bar{E}_M-\bar{E}_N}-\bar{Z}_M=\frac{\bar{K}\bar{Z}_\Sigma}{\bar{K}-1}-\bar{Z}_M=\lambda_r+j\lambda_i \tag{9}$$

$$Z_{op}=Z_R\frac{\lambda_r\cos\varphi_T+\lambda_i\sin\varphi_T}{\sqrt{\lambda_r^2+\lambda_i^2}} \tag{10}$$

The operation condition is given by (11), and expanded to (12), where $\eta=Z_M/Z_\Sigma$, $\mu=Z_R/Z_\Sigma$. It is possible to find the critical swing angle δ with given K by tracking the swing loci crossing the protection boundary, but it is very time-consuming.

$$Z_a-Z_{op}=\sqrt{\lambda_r^2+\lambda_i^2}-Z_R\frac{\lambda_r\cos\varphi_T+\lambda_i\sin\varphi_T}{\sqrt{\lambda_r^2+\lambda_i^2}}=0 \tag{11}$$

$$\left\{\frac{K^2\cos\varphi_\Sigma-K\cos(\delta+\varphi_\Sigma)}{K^2+1-2K\cos\delta}-\left(\eta\cos\varphi_M+\frac{\mu\cos\varphi_T}{2}\right)\right\}^2$$

$$+\left\{\frac{K^2\sin\varphi_\Sigma-K\sin(\delta+\varphi_\Sigma)}{K^2+1-2K\cos\delta}-\left(\eta\sin\varphi_M+\frac{\mu\sin\varphi_T}{2}\right)\right\}^2-\frac{\mu^2}{4}=0 \tag{12}$$

An alternative method is to find K with each possible critical angle δ. Therefore, the operation condition is expressed by a polynominal (13), with its coefficients m_i defined by (14)–(18). Its practical solution, a nonnegative real variable, is one of the roots for the polynominal.

$$m_4K^4+m_3K^3+m_2K^2+m_1K+m_0=0 \tag{13}$$

$$\begin{cases}m_0=c_1^2+c_2^2-c_3^2\\ m_1=2(b_1c_1+b_2c_2-b_3c_3)\\ m_2=b_1^2+b_2^2-b_3^2+2a_1c_1+2a_2c_2-2a_3c_3\\ m_3=2(a_1b_1+a_2b_2-a_3b_3)\\ m_4=a_1^2+a_2^2-a_3^2\end{cases} \tag{14}$$

$$\begin{cases}a_0=\eta\cos\varphi_M+\mu\cos\varphi_T/2\\ b_0=\eta\sin\varphi_M+\mu\sin\varphi_T/2\end{cases} \tag{15}$$

$$\begin{cases}a_1=\cos\varphi_\Sigma-a_0\\ b_1=2a_0\cos\delta-\cos(\delta+\varphi_\Sigma)\\ c_1=-a_0\end{cases} \tag{16}$$

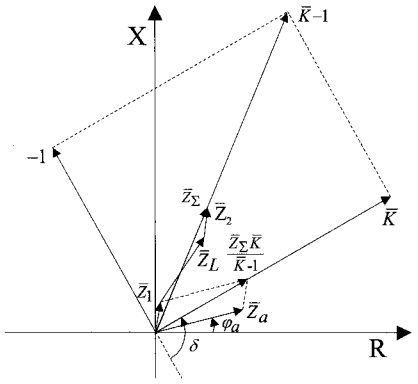

(a) δ>0

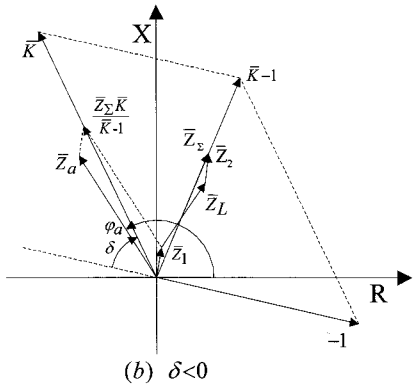

(b) δ<0

Fig. 4. Apparent impedance with source impedances

$$\begin{cases} a_2=\sin\varphi_\Sigma-b_0 \\ b_2=2b_0\cos\delta-\sin(\delta+\varphi_\Sigma) \\ c_2=-b_0 \end{cases} \tag{17}$$

$$\begin{cases} a_3=\mu K^2/2 \\ b_3=-\mu\cos\delta \\ c_3=\mu/2 \end{cases} \tag{18}$$

4.3 With source impedances and line charging

The line charging partially counteracts the voltage drop on the line impedance. It is negligible for low-voltage or short transmission lines, but obvious for long high-voltage lines. Based on the network equation in terms of nodal admittance matrix (19), the apparent impedance is given by (20). The operation condition in (21) is transformed to a polynominal (22), with its coefficients n_i defined by (23)–(27).

$$\begin{bmatrix} \frac{\bar{E}_M}{\bar{Z}_M} \\ \frac{\bar{E}_N}{\bar{Z}_N} \end{bmatrix}=\begin{bmatrix} \frac{1}{\bar{Z}_M}+\frac{1}{\bar{Z}_L}+j\frac{B}{2} & -\frac{1}{\bar{Z}_L} \\ -\frac{1}{\bar{Z}_L} & \frac{1}{\bar{Z}_N}+\frac{1}{\bar{Z}_L}+j\frac{B}{2} \end{bmatrix}\begin{bmatrix} \bar{E}_A \\ \bar{E}_B \end{bmatrix} \tag{19}$$

$$\bar{Z}_a=\frac{\bar{E}_A}{\bar{I}_L}=\frac{\bar{E}_A}{\frac{jB}{2}\bar{E}_A+\frac{\bar{E}_A-\bar{E}_B}{\bar{Z}_L}}=\frac{\left(\bar{Z}_L+\bar{Z}_N+j\frac{B}{2}\bar{Z}_L\bar{Z}_N\right)\bar{K}+\bar{Z}_M}{\left(\frac{jB}{2}\bar{Z}_L+jB\bar{Z}_N-\frac{B^2}{4}\bar{Z}_L\bar{Z}_N+1\right)\bar{K}-1}$$

$$=\frac{\left(f_2K^2+f_1K+f_0\right)+j\left(g_2K^2+g_1K+g_0\right)}{h_2K^2+h_1K+h_0} \tag{20}$$

$$Z_R\frac{\cos\varphi_{line}\left(f_2K^2+f_1K+f_0\right)+\sin\varphi_{line}\left(g_2K^2+g_1K+g_0\right)}{\sqrt{\left(f_2K^2+f_1K+f_0\right)^2+\left(g_2K^2+g_1K+g_0\right)^2}}$$

$$-\frac{\sqrt{\left(f_2K^2+f_1K+f_0\right)^2+\left(g_2K^2+g_1K+g_0\right)^2}}{h_2K^2+h_1K+h_0}=0 \tag{21}$$

$$n_4K^4+n_3K^3+n_2K^2+n_1K+n_0=0 \tag{22}$$

$$\begin{cases} e_1+je_2=\bar{Z}_L+\bar{Z}_N+jB\bar{Z}_L\bar{Z}_N/2 \\ e_3+je_4=\bar{Z}_M \\ e_5+je_6=jB\bar{Z}_L/2+jB\bar{Z}_N-B^2\bar{Z}_L\bar{Z}_N/4+1 \end{cases} \tag{23}$$

$$\begin{cases} f_2=e_1e_5+e_2e_6 \\ f_1=e_3e_5\cos\delta-e_3e_6\sin\delta+e_4e_6\cos\delta+e_4e_5\sin\delta \\ \quad +e_2\sin\delta-e_1\cos\delta \\ f_0=-e_3 \end{cases} \tag{24}$$

$$\begin{cases} g_2=e_2e_5-e_1e_6 \\ g_1=e_4e_5\cos\delta-e_4e_6\sin\delta-e_3e_6\cos\delta-e_3e_5\sin\delta \\ \quad -e_1\sin\delta-e_2\cos\delta \\ g_0=-e_4 \end{cases} \tag{25}$$

$$\begin{cases} h_2=e_5^2+e_6^2 \\ h_1=2e_6\sin\delta-2e_5\cos\delta \\ h_0=1 \end{cases} \tag{26}$$

$$\begin{cases} n_0=-f_0^2-g_0^2+Z_R\cos\varphi_T f_0h_0+Z_R\sin\varphi_T g_0h_0 \\ n_1=-2f_1f_0-2g_1g_0+Z_R\cos\varphi_T\left(f_1h_0+f_0h_1\right) \\ \quad +Z_R\sin\varphi_T\left(g_1h_0+g_0h_1\right) \\ n_2=Z_R\cos\varphi_T\left(f_2h_0+f_1h_1+f_0h_2\right)-2f_2f_0-2g_2g_0 \\ \quad +Z_R\sin\varphi_T\left(g_2h_0+g_1h_1+g_0h_2\right)-f_1^2-g_1^2 \\ n_3=-2f_2f_1-2g_2g_1+Z_R\cos\varphi_T\left(f_2h_1+f_1h_2\right) \\ \quad +Z_R\sin\varphi_T\left(g_2h_1+g_1h_2\right) \\ n_4=-f_2^2-g_2^2+Z_R\cos\varphi_T f_2h_2+Z_R\sin\varphi_T g_2h_2 \end{cases} \tag{27}$$

5. Numerical Analysis

For the system configuration given in Fig. 1, the line length is 80kM with rated voltage of 500 kV and rating power of 1000MVA. The per kM parameters are 0.018707Ω/kM, 0.87685mH/kM, and 13.351pF/kM. The source impedances at M and N side are 0.25+2.75i Ω and 0.50+4.50i Ω. The system frequency is 50 Hz. The base power in per unit system is 100MVA.

At first influence of MTA, source impedances, and shunt capacitance on the operation condition of the mho relay R1 is analyzed; then the critical swing frequency leading to relay operation is quantified.

5.1 Critical swing angle and influence of MTA

To quantify the influence of MTA, source impedances and line charging is ignored. The swing loci with different K are shown in Fig. 5, and the operation conditions with different MTA are given in Fig. 6. It is found:

(i) The swing loci traverse the protection region from the

right side of line impedance for a positive δ, or from the left side for a negative δ. Since the load angle is usually less than the line impedance angle, the critical positive δ is important for relays to withstand load encroachments and stable power swings.

(ii) In terms of swing angle, swing loci are more densely populated inside than outside of the protection region. If the swing frequency is approximately constant, the residence time inside the protection region may be long enough to activate the relay.

(iii) The operation region and the non-operation region can be clearly quantified by K–δ curve. When TA applies the 1.5 (line impedance angle), the relay operates when δ>0.2160 or δ<-0.2160 for K=1.04; it operates when δ>0.0945 or δ<-0.0945 for K=1.06; it wholly falls into the protection region, and operates at any δ for K>1.0648.

(iv) With K=1.06, when MTA=1.6, the relay will operate at δ>0.2346 or δ<-0.0406; when MTA=1.4, it will operate at δ>0.0391 or δ<-0.2451; when MTA=1.3, it will operate at δ>0.0265 or δ<-0.4325. Smaller MTA corresponds to smaller positive critical angle, and the relays may be more sensitive to load encroachments and stable power swings.

5.2 Influence of the source impedance

With the line impedance angle applied as TA, the apparent impedances and the operation condition are shown in Fig. 7 and Fig. 8. Compared with Fig. 5 and Fig. 6, it is found:

(i) The source impedances keep the swing loci far from the protection region, and make the relays less sensitive to power swings. For K=1.04, the critical δ is -0.3164 or 0.3371; for K=1.06, the critical δ is -0.2372 or 0.2579; only when K>1.0873 does the relay operate at any δ.

(ii) δ is 0.0094 at the peak of the non-operation region,

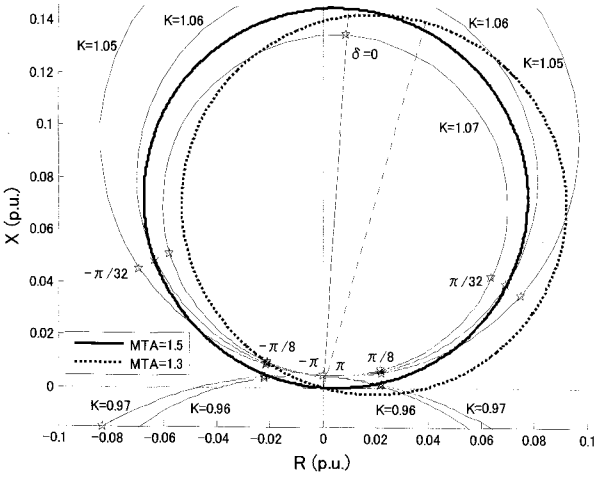

Fig. 5. Apparent impedance during power swing

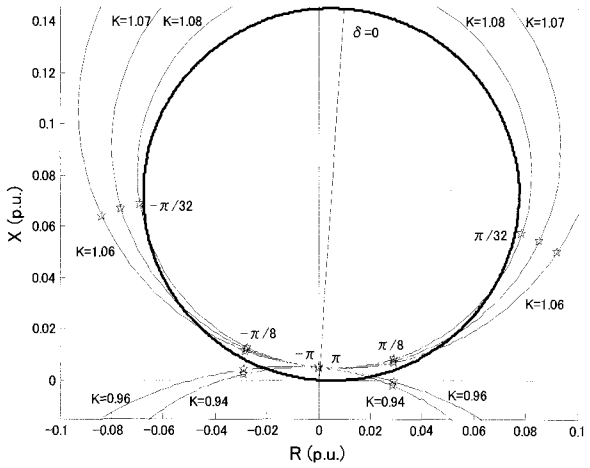

Fig. 7. Apparent impedance during power swing with source impedances

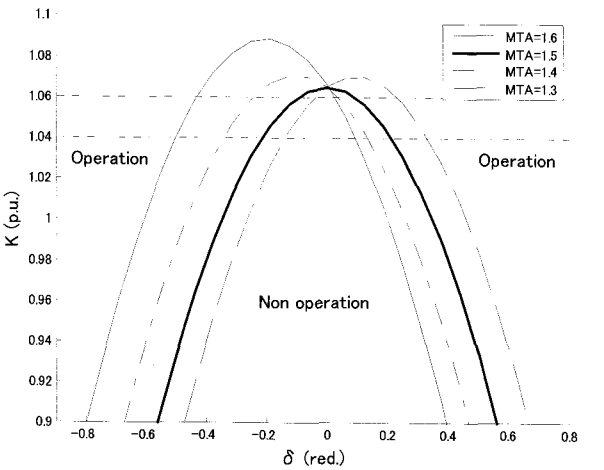

Fig. 6. Operation condition during power swing

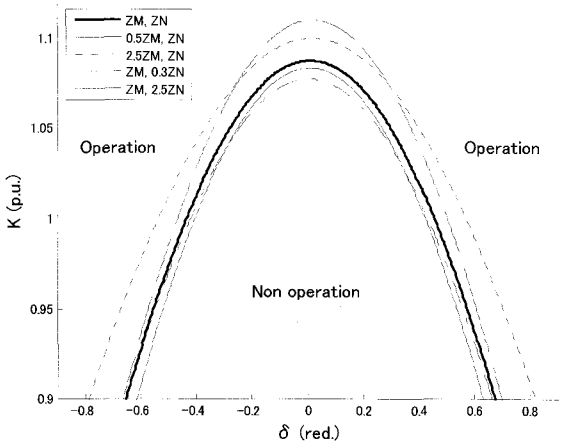

Fig. 8. Operation condition during power swing with source impedances

which shows the non-operation is no longer symmetrical in regards to the line impedance angle.

(iii) Greater source impedance yields larger non-operation region, and influence of the source impedance at the near end is more obvious than that at the far end.

5.3 Influence of the shunt capacitance

With the source impedances and the shunt capacitance, the swing loci are presented in Fig. 9, and the operation conditions with different line lengths are shown in Fig. 10. It is found that the non-operation regions increase with the line length. For example, with the length of 40 kM, the relay operates when $\delta<-0.1656$ or $\delta>0.1927$ for K=1.06; it operates at any δ for K>1.0734. With the length of 120 kM, the relay operates when $\delta<-0.3903$ or $\delta>0.4041$ for K=1.06; it operates at any δ for K>1.1375.

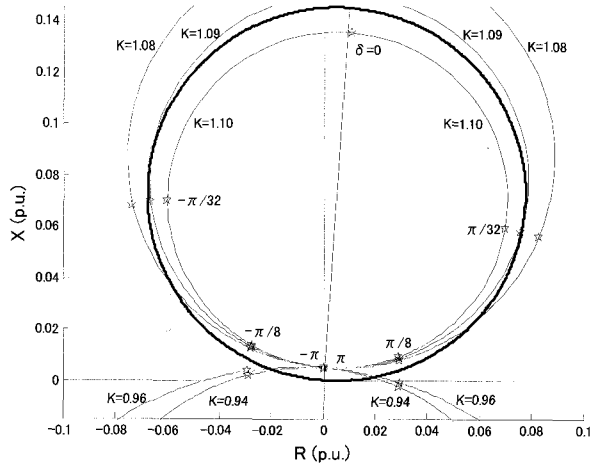

Fig. 9. Apparent impedance during power swing with source impedances and shunt capacitance

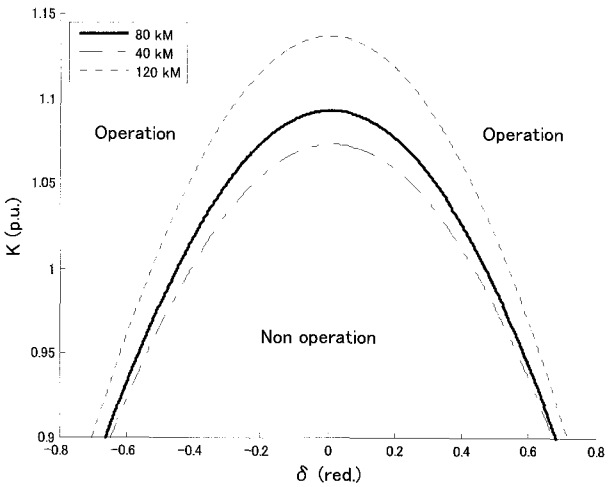

Fig. 10. Operation condition during power swing with source impedances and shunt capacitance

5.4 Critical swing frequency

Based on the critical swing angles in Fig. 10, the critical swing frequencies with respect to relays' time settings are shown in Fig. 11. It is found:

(i) Zone 3 relays with longer time setting are less sensitive to power swings, because they can only be activated by swings with lower frequency.

(ii) With a larger K, the critical swing frequency and the operation region increase, and the relays are more likely to operate.

(iii) For relays' time setting of 0.5-2.5s, the critical swing frequency is between 0.3268 Hz and 1.9446 Hz, which is in the range of low-frequency power swings.

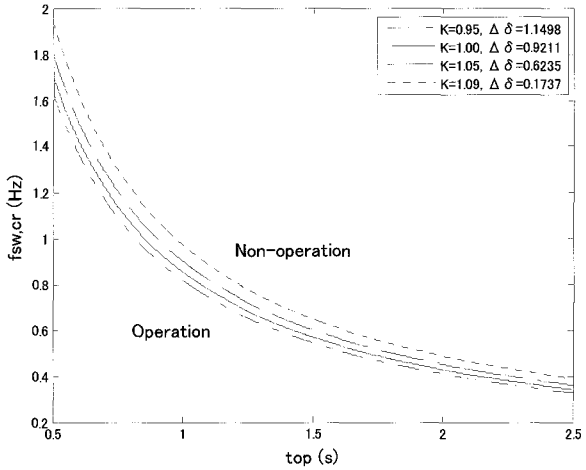

Fig. 11. Critical swing frequency viz. time setting of mho relays

6. Conclusions

In this paper, the performance of zone 3 impedance relays under power swings is studied. A new method is proposed to find the critical swing angle and the critical swing frequency for relay operation, which is applied to quantify the influence of relay setting and system conditions on the relay performance. The more elaborated parameters for the equivalent generators will improve the feasibility of the proposed method.

Some conclusions are outlined as follows:

(i) Although the swing loci inside the protection region are limited, the swing angles are more densely populated inside than outside of the protection region, and the residence time may be long enough to activate the relays.

(ii) The non-operation condition is dependent on relay settings and system parameters, which may make the relays sensitive to load encroachments and stable

power swings.

(iii) The critical frequency for relay operation is dependent on the time setting for the relays, and may be in the range of frequency of power swings.

Acknowledgements

This work was supported by the National Natural Science Foundation of China under Grant 50707006, and the Science and Technological Fund of Anhui Province for Outstanding Youth. Encouragements from Prof. N. Yorino and Y. Zoka at Hiroshima University, Japan, and Prof. M. Ding at the Research Center for Photovoltaic System Engineering, Ministry of Education, China, are gratefully acknowledged.

References

[1] M. Klein, G.J. Rogers, and P. Kundur, "A fundamental study of inter-area oscillations in power systems", *IEEE Trans. Power Syst.*, vol. 6, no. 3, pp. 914–921, Aug. 1991.

[2] D.N. Kosterev, C.W. Taylor, and W.A. Mittelstadt, "Model validation for the August 10, 1996 WSCC system outage", *IEEE Trans. Power Syst.*, vol. 14, no. 3, pp. 967–979, Aug. 1999.

[3] B. Yu, J. Sun, S. Tang, X. Wu, and H. Liang, "Analysis of low frequency oscillation in Hubei electric power system", *Automation of Electric Power Syst.*, vol. 25, no. 15, pp. 39–42, Aug. 2001.

[4] A. Mechraoui and D. W. P. Thomas, "A new blocking principle with phase and earth fault detection during fast power swings for distance protection", *IEEE Trans. Power Del.*, vol. 10, no. .3, pp. 1242–1248, July 1995.

[5] L. Zou, Q. Zhao, X. Lin, and P. Liu, "Improved phase selector for unbalanced faults during power swings using morphological technique", *IEEE Trans. Power Del.*, vol. 21, no. 4, pp. 1847–1855, Oct. 2006.

[6] IEEE PSRC. (2005). Power Swing and Out-of-Step Considerations on Transmission Lines. [Online]. Available: http://www.pes-psrc.org.

[7] S.H. Horowitz and A.G. Phadke, "Third zone revisited", *IEEE Trans. Power Del.*, vol. 21, no. 1, pp. 23–29, Jan. 2006.

[8] S. Li and M. Ding, "The vulnerability analysis of transmission system based on the performance of mho relay and SVC", *Int. J. Emerging Electric Power Syst.*, vol. 8, no. 1, 1–15, 2007.

[9] S. Li, N. Yorino, and Y. Zoka, "Controllability analysis for operation margin of zone 3 impedance relay", *IEEJ Trans. Power and Energy*, vol. 127, no. 3, 502–506, Mar. 2007.

[10] S. Li, N. Yorino, and Y. Zoka, "Operation margin analysis of zone 3 impedance relay based on sensitivities to power injection", *IET Gener. Transm. and Distrib.*, vol. 1, no. 2, pp. 312–317, Mar. 2007.

[11] NERC. (2005). Working Paper on a Proposed Transmission Relay Loadability Standard. [Online]. Available: http://www.nerc.com.

[12] AREVA-TD, PRAG Network Protection & Automation Guide. [Online]. Available: http://www.areva-td.com.

[13] D. Tziouvaras. Relay Performance during Major System Disturbances. [Online]. Available: www.selinc. com.

[14] G. Gangadharan and A. Anbalagan, "Microprocessor based three step quadrilateral distance relay for the protection of EHV/UHV transmission line", *IEEE Trans. Power Del.*, vol. 7, no. 1, pp. 91–97, Jan. 1992.

[15] J. He, Y. Li, B. Li, Z. Guo, and X. Dong, "Relay protection for UHV transmission lines, part II disposition of relay protection", *Automation of Electric Power Syst.*, vol. 26, no. 24, pp. 1–6, Dec. 2002.

Shenghu Li

He received his B.Sc., M.Sc., and Ph.D. degrees in Electrical Engineering from the Hefei University of Technology, Hefei, China in 1995, 2000 and 2003, respectively. Currently, he is an Associate Professor at the School of Electrical Engineering and its Automation, Hefei University of Technology, China. He joined the Research Center for Photovoltaic System Engineering, Ministry of Education, China, in 2002. He was a Postdoctoral Researcher at Hiroshima University, Japan, from 2005 to 2007. He was the recipient of the Xuji Award (2nd prize) from the China Association of Education of Electric Power, in 2002, and the Natural Science Award of Anhui Province (2nd prize, 2nd contributor), in 2004. His research interests are power system security and FACTS. He is a member of IEEE and the Chinese Society for Electrical Engineering (CSEE).